SIAM J. SCI. COMPUT.
Vol. 36, No. 4, pp. A2023–A2046

A DIRECT SOLVER WITH $O(N)$ COMPLEXITY FOR VARIABLE COEFFICIENT ELLIPTIC PDES DISCRETIZED VIA A HIGH-ORDER COMPOSITE SPECTRAL COLLOCATION METHOD*

A. GILLMAN† AND P. G. MARTINSSON‡

Abstract. A numerical method for solving elliptic PDEs with variable coefficients on two-dimensional domains is presented. The method is based on high-order composite spectral approximations and is designed for problems with smooth solutions. The resulting system of linear equations is solved using a direct (as opposed to iterative) solver that has optimal $O(N)$ complexity for all stages of the computation when applied to problems with nonoscillatory solutions such as the Laplace and the Stokes equations. Numerical examples demonstrate that the scheme is capable of computing solutions with a relative accuracy of 10^{-10} or better for challenging problems such as highly oscillatory Helmholtz problems and convection-dominated convection-diffusion equations. In terms of speed, it is demonstrated that a problem with a nonoscillatory solution that was discretized using 10^8 nodes can be solved in 115 minutes on a personal workstation with two quad-core 3.3 GHz CPUs. Since the solver is direct, and the "solution operator" fits in RAM, any solves beyond the first are very fast. In the example with 10^8 unknowns, solves require only 30 seconds.

Key words. fast direct solver, high-order discretization, multidomain spectral method, nested dissection, multifrontal method, structured matrix algebra, hierarchically block separable matrix, reduction to interface, Dirichlet-to-Neumann operator, Poincaré–Steklov operator

AMS subject classification. 65N35

DOI. 10.1137/130918988

1. Introduction.

1.1. Problem formulation.

The paper describes a numerical method with optimal $O(N)$ complexity for solving boundary value problems of the form

$$\begin{cases} Au(\boldsymbol{x}) = 0 & \boldsymbol{x} \in \Omega, \\ u(\boldsymbol{x}) = f(\boldsymbol{x}) & \boldsymbol{x} \in \Gamma, \end{cases} \tag{1}$$

where Ω is a rectangle in the plane with boundary Γ, and where A is a coercive elliptic partial differential operator

$$\begin{aligned}[Au](\boldsymbol{x}) = &-c_{11}(\boldsymbol{x})[\partial_1^2 u](\boldsymbol{x}) - 2c_{12}(\boldsymbol{x})[\partial_1\partial_2 u](\boldsymbol{x}) - c_{22}(\boldsymbol{x})[\partial_2^2 u](\boldsymbol{x}) \\ &+ c_1(\boldsymbol{x})[\partial_1 u](\boldsymbol{x}) + c_2(\boldsymbol{x})[\partial_2 u](\boldsymbol{x}) + c(\boldsymbol{x})\, u(\boldsymbol{x}).\end{aligned} \tag{2}$$

The methodology is based on a high-order composite spectral discretization and can be modified to handle a range of different domains, including curved ones. For problems with smooth solutions, we demonstrate that the method can easily produce answers with ten or more correct digits.

*Submitted to the journal's Methods and Algorithms for Scientific Computing section April 30, 2013; accepted for publication (in revised form) May 27, 2014; published electronically August 29, 2014. The work was supported by NSF awards DMS-0748488 and CDI-0941476, and by DARPA award N66001-13-1-4050.

http://www.siam.org/journals/sisc/36-4/91898.html

†Department of Mathematics, Dartmouth College, Hanover, NH 03755 (adrianna.gillman@dartmouth.edu).

‡Department of Applied Mathematics, University of Colorado at Boulder, Boulder, CO 80309 (martinss@colorado.edu).

The proposed method is based on a *direct solver* which in a single sweep constructs an approximation to the solution operator of (1). This gives the solver several advantages over established linear complexity methods based on *iterative solvers* (e.g., GMRES or multigrid); perhaps, most importantly, the new method can solve problems for which iterative methods converge slowly or not at all. The direct solver has $O(N)$ complexity for all stages of the computation. A key feature is that once the solution operator has been built, solves can be executed extremely rapidly, making the scheme excel when solving a sequence of equations with the same operator but different boundary data.

1.2. Outline of solution procedure. The method in this paper is comprised of three steps.

1. The domain is first tessellated into a hierarchical tree of rectangular patches. For each patch on the finest level, a local "solution operator" is built using a dense brute force calculation. The "solution operator" will be defined in section 1.3; for now we simply note that it encodes all information about the patch that is required to evaluate interactions with other patches.
2. The larger patches are processed in an upwards pass through the tree, where each parent can be processed once its children have been processed. The processing of a parent node consists of forming its solution operator by "gluing together" the solution operators of its children.
3. Once the solution operators for all patches have been computed, a solution to the PDE can be computed via a downwards pass through the tree. This step is typically *very* fast.

1.3. Local solution operators. The "local solution operators" introduced in section 1.2 take the form of discrete approximations to the *Dirichlet-to-Neumann*, or "DtN," maps. To explain what these maps do, first observe that for a given boundary function f, the BVP (1) has a unique solution u (recall that we assume A to be coercive). For $\boldsymbol{x} \in \Gamma$, let $g(\boldsymbol{x}) = u_n(\boldsymbol{x})$ denote the normal derivative in the outwards direction of u at $\boldsymbol{x}$. The process for constructing the function g from f is linear, we write it as

$$g = T\, f.$$

Or, equivalently,

$$T:\ u|_\Gamma \mapsto u_n|_\Gamma, \quad \text{where } u \text{ satisfies } Au = 0 \text{ in } \Omega.$$

From a mathematical perspective, the map T is a slightly unpleasant object; it is a hypersingular integral operator whose kernel exhibits complicated behavior near the corners of Γ. A key observation is that in the present context, these difficulties can be ignored since we limit attention to functions that are smooth. In a sense, we only need to accurately represent the projection of the "true" operator T onto a space of smooth functions (that in particular do not have any corner singularities).

Concretely, given a square box Ω_τ we represent a boundary potential $u|_\Gamma$ and a boundary flux $u_n|_\Gamma$ via tabulation at a set of r tabulation points on each side. (For a leaf box, we use r Gaussian nodes.) The DtN operator T^τ is then represented simply as a dense matrix $\mathbf{T}^\tau$ of size $4r \times 4r$ that maps tabulated boundary potentials to the corresponding tabulated boundary fluxes.

1.4. Computational complexity. A straightforward implementation of the direct solver outlined in sections 1.2 and 1.3 in which all solution operators $\mathbf{T}^\tau$ are

treated as general dense matrices has asymptotic complexity $O(N^{3/2})$ for the "build stage" where the solution operators are constructed, and $O(N \log N)$ complexity for the "solve stage" where the solution operator is applied for a given set of boundary data [19]. This paper demonstrates that by exploiting internal structure in these operators, they can be stored and manipulated efficiently, resulting in optimal $O(N)$ overall complexity.

To be precise, the internal structure exploited is that the off-diagonal blocks of the dense solution operators can to high accuracy be approximated by matrices of low rank. This property is a result of the fact that for a patch Ω_τ, the matrix $\mathbf{T}^\tau$ is a discrete approximation of the continuum DtN operator T^τ, which is an integral operator whose kernel is smooth away from the diagonal.

Remark 1.1. The proposed solver can also handle noncoercive problems such as the Helmholtz equation. If the equation is kept fixed while N is increased, $O(N)$ complexity is retained. (A slight complication arises in that the DtN operator does not always exist, but this can be rectified by considering other Poincaré–Steklov operators, such as, e.g., the impedance-to-impedance map; see [9].) However, in the context of elliptic problems with oscillatory solutions, it is common to scale N to the wavelength so that the number of discretization points per wavelength is fixed as N increases. Our accelerated technique will in this situation lead to a practical speed-up, but will have the same $O(N^{3/2})$ asymptotic scaling as the basic method that does not use fast operator algebra.

1.5. Prior work. The direct solver outlined in section 1.2 is an evolution of a sequence of direct solvers for integral equations dating back to [20] and later [11, 10, 12, 3, 4]. The common idea is to build a global solution operator by splitting the domain into a hierarchical tree of patches, build a local solution operator for each "leaf" patch, and then build solution operators for larger patches via a hierarchical merge procedure in a sweep over the tree from smaller to larger patches. In the context of integral equations, the "solution operator" is a type of scattering matrix, while in the present context, the solution operator is a DtN operator.

The direct solvers [20, 11, 10, 12, 3], designed for dense systems, are conceptually related to earlier work on direct solvers for sparse systems arising from finite difference and finite element discretizations of elliptic PDEs such as the classical nested dissection method of George [7, 13] and the multifrontal methods by Duff, Erisman, and Reid [6]. Conceptually, these solvers can be viewed as hierarchical versions of the classical "static condensation" idea in finite element analysis [25]. These techniques typically require $O(N^{3/2})$ operations to construct the LU-factorization of a sparse coefficient matrix arising from the discretization of an elliptic PDE on a planar domain, with the dominant cost being the formation of Schur complements and LU-factorizations of dense matrices of size up to $O(N^{0.5}) \times O(N^{0.5})$. It was demonstrated in the last several years that these dense matrices have internal structure that allows the direct solver to be accelerated to linear or close to linear complexity; see, e.g., [26, 8, 16, 17, 22]. These accelerated nested dissection methods are closely related to the fast direct solver presented in this manuscript, and served as an inspiration for our work. An important difference is that the method in the present paper allows high-order discretizations to be used without increasing the cost of the direct solver. To be technical, the solvers in [26, 8, 16, 17, 22] are based on an underlying finite difference or finite element discretization. High-order discretization in this context tends to lead to large frontal matrices (since the "dividers" that partition the grid get wider as the order increases), and consequently very high cost of the LU-factorization (see, e.g., Table 3).

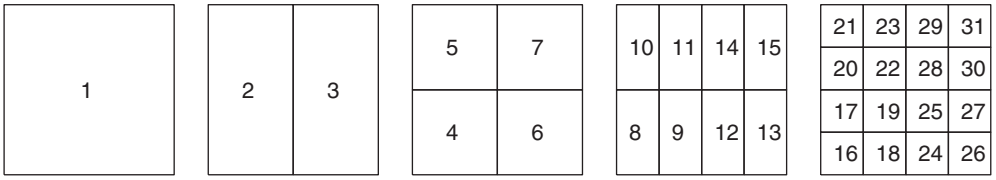

FIG. 1. *The square domain Ω is split into 4×4 leaf boxes. These are then gathered into a binary tree of successively larger boxes as described in section* 5.1. *One possible enumeration of the boxes in the tree is shown, but note that the only restriction is that if box τ is the parent of box σ, then $\tau < \sigma$.*

Our discretization scheme is related to earlier work on spectral collocation methods on composite ("multidomain") grids, such as, e.g., [15, 27], and, in particular, Pfeiffer et al. [21]. For a detailed review of the similarities and differences, see [19]. The procedure is conceptually related to so-called "reduction to the interface" methods; see [14] and the references therein. These "interface" methods also use local solution operators defined on boundaries (often referred to as "discrete Poincaré–Steklov operators") but typically discretize a variational problem instead of the PDE directly.

1.6. Novelty of the proposed method. A solver with $O(N^{3/2})$ complexity based on the idea of hierarchical construction of DtN maps was previously described in [19], which in turn is based on [18]. The principal contribution of the present work is a technique that exploits internal structure in the dense matrices representing DtN maps to improve on the computational complexity from $O(N^{3/2})$ to $O(N)$. The acceleration technique was inspired by similar ideas presented in [26, 8, 16, 17, 22].

In addition to the improvement in complexity, the paper also describes a new representation of the local solution operators that leads to cleaner implementation of the direct solvers and allows greater flexibility in executing the leaf computation; see Remark 3.1.

1.7. Outline of paper. Section 2 introduces the mesh of Gaussian nodes that forms our basic computational grid. Sections 3, 4, and 5 describe a relatively simple direct solver with $O(N^{3/2})$ complexity. Sections 6, 7, and 8 describe how to improve the asymptotic complexity of the direct solver from $O(N^{3/2})$ to $O(N)$ by exploiting internal structure in certain dense matrices. Section 9 describes numerical examples and section 10 summarizes the key findings.

2. Discretization. Partition the domain Ω into a collection of square (or possibly rectangular) boxes, called *leaf boxes*. On the edges of each leaf, place q Gaussian interpolation points. The size of the leaf boxes, and the parameter q should be chosen so that any potential solution u of (1), as well as its first and second derivatives, can be accurately interpolated from their values at these points ($q = 21$ is often a good choice). Let $\{\boldsymbol{x}_k\}_{k=1}^N$ denote the collection of interpolation points on all boundaries.

Next construct a binary tree on the collection of leaf boxes by hierarchically merging them, making sure that all boxes on the same level are roughly of the same size; cf. Figure 1. The boxes should be ordered so that if τ is a parent of a box σ, then $\tau < \sigma$. We also assume that the root of the tree (i.e., the full box Ω) has index $\tau = 1$. We let Ω_τ denote the domain associated with box τ.

With each box τ, we define two index vectors I_{i}^τ and I_{e}^τ as follows:

I_{e}^τ A list of all *exterior* nodes of τ. In other words, $k \in I_{\mathrm{e}}^\tau$ iff $\boldsymbol{x}_k$ lies on the boundary of Ω_τ.

I_{i}^{τ} For a parent τ, I_{i}^{τ} is a list of all its *interior* nodes that are not interior nodes of its children. For a leaf τ, I_{i}^{τ} is empty.

Let $\mathbf{u} \in \mathbb{R}^N$ denote a vector holding approximations to the values of u of (1), in other words,

$$\mathbf{u}(k) \approx u(\boldsymbol{x}_k).$$

Finally, let $\mathbf{v} \in \mathbb{R}^N$ denote a vector holding approximations to the boundary fluxes of the solution u of (1), in other words,

$$\mathbf{v}(k) \approx \begin{cases} \partial_2 u(\boldsymbol{x}_k), & \text{when } \boldsymbol{x}_j \text{ lies on a horizontal edge,} \\ \partial_1 u(\boldsymbol{x}_k), & \text{when } \boldsymbol{x}_j \text{ lies on a vertical edge.} \end{cases}$$

Note the $\mathbf{v}(k)$ represents an *outgoing flux* on certain boxes and an *incoming flux* on others. This is a deliberate choice to avoid problems with signs when matching fluxes of touching boxes.

3. Constructing the Dirichlet-to-Neumann map for a leaf. This section describes a spectral method for computing a discrete approximation to the DtN map T^{τ} associated with a leaf box Ω_{τ}. In other words, if u is a solution of (1), we seek a matrix $\mathbf{T}^{\tau}$ of size $4q \times 4q$ such that

$$\mathbf{v}(I_{\mathrm{e}}^{\tau}) \approx \mathbf{T}^{\tau}\, \mathbf{u}(I_{\mathrm{e}}^{\tau}). \tag{3}$$

Conceptually, we proceed as follows: Given a vector $\mathbf{u}(I_{\mathrm{e}}^{\tau})$ of potential values tabulated on the boundary of Ω_{τ}, form for each side the unique polynomial of degree at most $q-1$ that interpolates the q specified values of u. This yields Dirichlet boundary data on Ω_{τ} in the form of four polynomials. Solve the restriction of (1) to Ω_{τ} for the specified boundary data using a spectral method on a local tensor product grid of $p \times p$ *Chebyshev nodes.* The vector $\mathbf{v}(I_{\mathrm{e}}^{\tau})$ is obtained by spectral differentiation of the local solution, and then retabulating the boundary fluxes to the Gaussian nodes in $\{\boldsymbol{x}_k\}_{k \in I_{\mathrm{e}}^{\tau}}$.

We give details of the construction in section 3.2, but as a preliminary step, we first review a classical spectral collocation method for the local solve in section 3.1

Remark 3.1. Chebyshev nodes are ideal for the leaf computations, and it is in principle also possible to use Chebyshev nodes to represent all boundary-to-boundary "solution operators" such as, e.g., $\mathbf{T}^{\tau}$ (indeed, this was the approach taken in the first implementation of the proposed method [19]). However, there are at least two substantial benefits to using Gaussian nodes that justify the trouble of retabulating the operators. First, the procedure for merging boundary operators defined for neighboring boxes is much cleaner and involves less bookkeeping since the Gaussian nodes do not include the corner nodes. (Contrast section 4 of [19] with section 4.) Second, and more importantly, the use of the Gaussian nodes allows for interpolation between different discretizations. Thus the method can easily be extended to have local refinement when necessary; see Remark 5.2.

3.1. Spectral discretization. Let Ω_{τ} denote a rectangular subset of Ω with boundary Γ_{τ}, and consider the local Dirichlet problem

$$[Au](\boldsymbol{x}) = 0, \qquad \boldsymbol{x} \in \Omega_{\tau}, \tag{4}$$

$$u(\boldsymbol{x}) = h(\boldsymbol{x}), \qquad \boldsymbol{x} \in \Gamma_{\tau}, \tag{5}$$

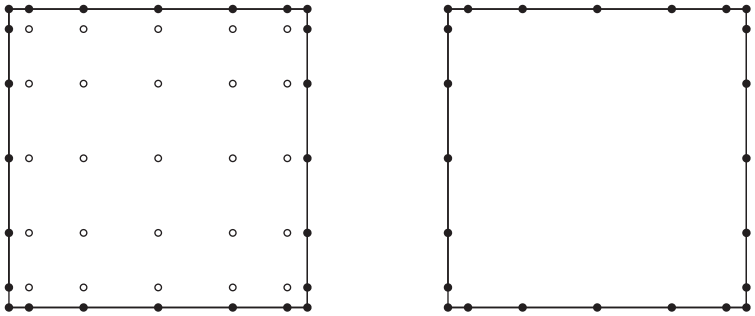

(a) (b)

FIG. 2. *Notation for the leaf computation in section* 3. (a) *A leaf before elimination of interior (white) nodes.* (b) *A leaf after elimination of interior nodes.*

where the elliptic operator A is defined by (2). We will construct an approximate solution to (4) using a classical spectral collocation method described in, e.g., Trefethen [24]: First, pick a small integer p and let $\{\boldsymbol{z}_k\}_{k=1}^{p^2}$ denote the nodes in a tensor product grid of $p \times p$ Chebyshev nodes on Ω_τ. Let $\mathbf{D}^{(1)}$ and $\mathbf{D}^{(2)}$ denote spectral differentiation matrices corresponding to the operators $\partial/\partial x_1$ and $\partial/\partial x_2$, respectively. The operator (2) is then locally approximated via the $p^2 \times p^2$ matrix

$$\mathbf{A} = -\mathbf{C}_{11}\big(\mathbf{D}^{(1)}\big)^2 - 2\mathbf{C}_{12}\mathbf{D}^{(1)}\mathbf{D}^{(2)} - \mathbf{C}_{22}\big(\mathbf{D}^{(2)}\big)^2 + \mathbf{C}_1\mathbf{D}^{(1)} + \mathbf{C}_2\mathbf{D}^{(2)} + \mathbf{C}, \tag{6}$$

where $\mathbf{C}_{11}$ is the diagonal matrix with diagonal entries $\{c_{11}(\boldsymbol{z}_k)\}_{k=1}^{p^2}$, and the other matrices $\mathbf{C}_{ij}$, $\mathbf{C}_i$, $\mathbf{C}$ are defined analogously.

Let $\mathbf{w} \in \mathbb{R}^{p^2}$ denote a vector holding the desired approximate solution of (4). We populate all entries corresponding to boundary nodes with the Dirichlet data from h, and then enforce a spectral collocation condition at the interior nodes. To formalize, let us partition the index set

$$\{1, 2, \ldots, p^2\} = J_{\mathrm{e}} \cup J_{\mathrm{i}}$$

in such a way that J_{e} contains the $4(p-1)$ nodes on the boundary of Ω_τ, and J_{i} denotes the set of $(p-2)^2$ interior nodes; see Figure 2(a). Then partition the vector $\mathbf{w}$ into two parts corresponding to internal and exterior nodes via

$$\mathbf{w}_{\mathrm{i}} = \mathbf{w}(J_{\mathrm{i}}), \quad \mathbf{w}_{\mathrm{e}} = \mathbf{w}(J_{\mathrm{e}}).$$

Analogously, partition $\mathbf{A}$ into four parts via

$$\mathbf{A}_{\mathrm{i,i}} = \mathbf{A}(J_{\mathrm{i}}, J_{\mathrm{i}}), \quad \mathbf{A}_{\mathrm{i,e}} = \mathbf{A}(J_{\mathrm{i}}, J_{\mathrm{e}}), \quad \mathbf{A}_{\mathrm{e,i}} = \mathbf{A}(J_{\mathrm{e}}, J_{\mathrm{i}}), \quad \mathbf{A}_{\mathrm{e,e}} = \mathbf{A}(J_{\mathrm{e}}, J_{\mathrm{e}}).$$

The potential at the exterior nodes is now given directly from the boundary condition

$$\mathbf{w}_{\mathrm{e}} = [h(\boldsymbol{z}_k)]_{k \in J_{\mathrm{e}}}.$$

For the internal nodes, we enforce the PDE (4) via direct collocation:

$$\mathbf{A}_{\mathrm{i,i}}\,\mathbf{w}_{\mathrm{i}} + \mathbf{A}_{\mathrm{i,e}}\,\mathbf{w}_{\mathrm{e}} = \mathbf{0}. \tag{7}$$

Solving (7) for $\mathbf{w}_{\mathrm{i}}$, we find

$$\mathbf{w}_{\mathrm{i}} = -\mathbf{A}_{\mathrm{i,i}}^{-1}\,\mathbf{A}_{\mathrm{i,e}}\,\mathbf{w}_{\mathrm{e}}. \tag{8}$$

3.2. Constructing the approximate DtN. Now that we know how to approximately solve the local Dirichlet problem (4) via a local spectral method, we can build a matrix $\mathbf{T}^\tau$ such that (3) holds to high accuracy. The starting point is a vector $\mathbf{u}(I_\tau) \in \mathbb{R}^{4q}$ of tabulated potential values on the boundary of Ω_τ. We will construct the vector $\mathbf{v}(I_\tau) \in \mathbb{R}^{4q}$ via four linear maps. The combination of these maps is the matrix $\mathbf{T}^\tau$. We henceforth assume that the spectral order of the local Chebyshev grid matches the order of the tabulation on the leaf boundaries so that $p = q$.

Step 1: *retabulation from Gaussian nodes to Chebyshev nodes.* For each side of Ω_τ, form the unique interpolating polynomial of degree at most $q-1$ that interpolates the q potential values on that side specified by $\mathbf{u}(I_{\mathrm{e}}^\tau)$. Now evaluate these polynomials at the boundary nodes of a $q \times q$ Chebyshev grid on Ω_τ. Observe that for a corner node, we may in the general case get conflicts. For instance, the potential at the southwest corner may get one value from extrapolation of potential values on the south border, and one value from extrapolation of the potential values on the west border. We resolve such conflicts by assigning the corner node the average of the two possibly different values. (In practice, essentially no error occurs since we know that the vector $\mathbf{u}(I_{\mathrm{e}}^\tau)$ tabulates an underlying function that is continuous at the corner.)

Step 2: *spectral solve.* Step 1 populates the boundary nodes of the $q \times q$ Chebyshev grid with Dirichlet data. Now determine the potential at all interior points on the Chebyshev grid by executing a local spectral solve; cf. (8).

Step 3: spectral differentiation. After Step 2, the potential is known at all nodes on the local Chebyshev grid. Now perform spectral differentiation to evaluate approximations to $\partial u/\partial x_2$ for the Chebyshev nodes on the two horizontal sides, and $\partial u/\partial x_1$ for the Chebyshev nodes on the two vertical sides.

Step 4: *retabulation from the Chebyshev nodes back to Gaussian nodes.* After Step 3, the boundary fluxes on $\partial\Omega_\tau$ are specified by four polynomials of degree $q-1$ (specified via tabulation on the relevant Chebyshev nodes). Now simply evaluate these polynomials at the Gaussian nodes on each side to obtain the vector $\mathbf{v}(I_{\mathrm{e}}^\tau)$.

Putting everything together, we find that the matrix $\mathbf{T}^\tau$ is given as a product of four matrices

$$\underset{4q\times 4q}{\mathbf{T}^\tau} = \underset{4q\times 4q}{\mathbf{L}_4} \circ \underset{4q\times q^2}{\mathbf{L}_3} \circ \underset{q^2\times 4(q-1)}{\mathbf{L}_2} \circ \underset{4(q-1)\times 4q}{\mathbf{L}_1},$$

where $\mathbf{L}_i$ is the linear transform corresponding to "Step i" above. Observe that many of these transforms are far from dense, for instance, $\mathbf{L}_1$ and $\mathbf{L}_4$ are 4×4 block matrices with all off-diagonal blocks equal to zero. Exploiting these structures substantially accelerates the computation.

Remark 3.2. The grid of Chebyshev nodes $\{\boldsymbol{z}_k\}_{j=1}^{p^2}$ introduced in section 3.1 is only used for the local computation. In the final solver, there is no need to store potential values at these grid points—they are used merely for constructing the matrix $\mathbf{T}^\tau$.

4. Merging two DtN maps. Let τ denote a box in the tree with children α and β. In this section, we demonstrate that if the DtN matrices $\mathbf{T}^\alpha$ and $\mathbf{T}^\beta$ for the children are known, then the DtN matrix $\mathbf{T}^\tau$ can be constructed via a purely local computation which we refer to as a "merge" operation.

We start by introducing some notation: Let Ω_τ denote a box with children Ω_α and Ω_β. For concreteness, let us assume that Ω_α and Ω_β share a vertical edge as shown in Figure 3, so that

$$\Omega_\tau = \Omega_\alpha \cup \Omega_\beta.$$

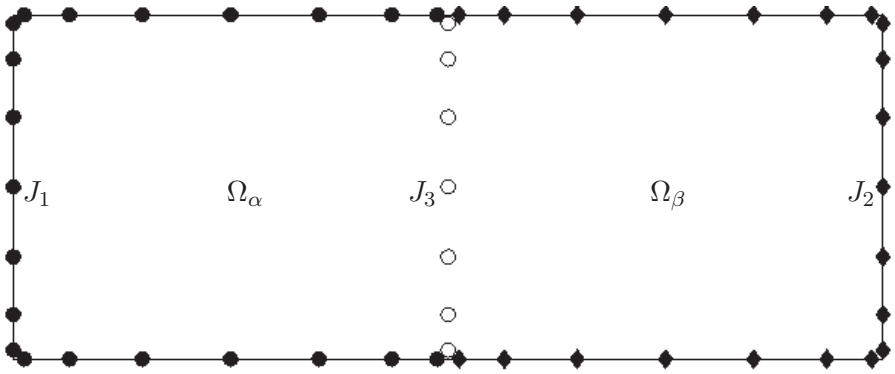

FIG. 3. *Notation for the merge operation described in section 4. The rectangular domain Ω is formed by two squares Ω_α and Ω_β. The sets J_1 and J_2 form the exterior nodes (black), while J_3 consists of the interior nodes (white).*

We partition the points on $\partial\Omega_\alpha$ and $\partial\Omega_\beta$ into three sets:

- J_1 Boundary nodes of Ω_α that are not boundary nodes of Ω_β.
- J_2 Boundary nodes of Ω_β that are not boundary nodes of Ω_α.
- J_3 Boundary nodes of both Ω_α and Ω_β that are *not* boundary nodes of the union box Ω_τ.

Figure 3 illustrates the definitions of the J_k's. Let u denote a solution to (1), with tabulated potential values $\mathbf{u}$ and boundary fluxes $\mathbf{v}$, as described in section 2. Since the interior and exterior nodes of τ are $I_i^\tau = J_3$ and $I_e^\tau = J_1 \cup J_3$, respectively, we set

$$\mathbf{u}_\mathrm{i} = \mathbf{u}_3 \qquad \text{and} \qquad \mathbf{u}_\mathrm{e} = \begin{bmatrix} \mathbf{u}_1 \\ \mathbf{u}_2 \end{bmatrix}. \tag{9}$$

Recall that $\mathbf{T}^\alpha$ and $\mathbf{T}^\beta$ denote the operators that map values of the potential u on the boundary to values of $\partial_n u$ on the boundaries of the boxes Ω_α and Ω_β, as described in section 3. The operators can be partitioned according to the numbering of nodes in Figure 3, resulting in the equations

$$\begin{bmatrix} \mathbf{v}_1 \\ \mathbf{v}_3 \end{bmatrix} = \begin{bmatrix} \mathbf{T}^\alpha_{1,1} & \mathbf{T}^\alpha_{1,3} \\ \mathbf{T}^\alpha_{3,1} & \mathbf{T}^\alpha_{3,3} \end{bmatrix} \begin{bmatrix} \mathbf{u}_1 \\ \mathbf{u}_3 \end{bmatrix} \qquad \text{and} \qquad \begin{bmatrix} \mathbf{v}_2 \\ \mathbf{v}_3 \end{bmatrix} = \begin{bmatrix} \mathbf{T}^\beta_{2,2} & \mathbf{T}^\beta_{2,3} \\ \mathbf{T}^\beta_{3,2} & \mathbf{T}^\beta_{3,3} \end{bmatrix} \begin{bmatrix} \mathbf{u}_2 \\ \mathbf{u}_3 \end{bmatrix}. \tag{10}$$

Our objective is now to construct a solution operator $\mathbf{S}^\tau$ and a DtN matrix $\mathbf{T}^\tau$ such that

$$\mathbf{u}_3 = \mathbf{S}^\tau \begin{bmatrix} \mathbf{u}_1 \\ \mathbf{u}_2 \end{bmatrix}, \tag{11}$$

$$\begin{bmatrix} \mathbf{v}_1 \\ \mathbf{v}_2 \end{bmatrix} = \mathbf{T}^\tau \begin{bmatrix} \mathbf{u}_1 \\ \mathbf{u}_2 \end{bmatrix}. \tag{12}$$

To this end, we write (10) as a single equation:

$$\left[\begin{array}{cc|c} \mathbf{T}^\alpha_{1,1} & \mathbf{0} & \mathbf{T}^\alpha_{1,3} \\ \mathbf{0} & \mathbf{T}^\beta_{2,2} & \mathbf{T}^\beta_{2,3} \\ \hline \mathbf{T}^\alpha_{3,1} & -\mathbf{T}^\beta_{3,2} & \mathbf{T}^\alpha_{3,3} - \mathbf{T}^\beta_{3,3} \end{array}\right] \left[\begin{array}{c} \mathbf{u}_1 \\ \mathbf{u}_2 \\ \hline \mathbf{u}_3 \end{array}\right] = \left[\begin{array}{c} \mathbf{v}_1 \\ \mathbf{v}_2 \\ \hline \mathbf{0} \end{array}\right]. \tag{13}$$

The last equation directly tells us that (11) holds with

$$\mathbf{S}^\tau = \left(\mathbf{T}^\alpha_{3,3} - \mathbf{T}^\beta_{3,3}\right)^{-1}\left[-\mathbf{T}^\alpha_{3,1} \mid \mathbf{T}^\beta_{3,2}\right]. \tag{14}$$

By eliminating $\mathbf{u}_3$ from (13) by forming a Schur complement, we also find that (12) holds with

$$\mathbf{T}^\tau = \begin{bmatrix} \mathbf{T}^\alpha_{1,1} & \mathbf{0} \\ \mathbf{0} & \mathbf{T}^\beta_{2,2} \end{bmatrix} + \begin{bmatrix} \mathbf{T}^\alpha_{1,3} \\ \mathbf{T}^\beta_{2,3} \end{bmatrix} \left(\mathbf{T}^\alpha_{3,3} - \mathbf{T}^\beta_{3,3}\right)^{-1}\left[-\mathbf{T}^\alpha_{3,1} \mid \mathbf{T}^\beta_{3,2}\right]. \tag{15}$$

5. The full hierarchical scheme. At this point, we know how to construct the DtN operator for a leaf (section 3), and how to merge two such operators of neighboring patches to form the DtN operator of their union (section 4). We are ready to describe the full hierarchical scheme for solving the Dirichlet problem (1). This scheme takes the Dirichlet boundary data f, and constructs an approximation to the solution u. The output is a vector $\mathbf{u}$ that tabulates approximations to u at the Gaussian nodes $\{\boldsymbol{x}_k\}_{k=1}^N$ on all interior edges that were defined in section 2. To find u at an arbitrary set of target points in Ω, a postprocessing step described in section 5.3 can be used.

5.1. The algorithm. Partition the domain into a hierarchical tree as described in section 2. Then execute a "build stage" in which we construct for each box τ the following two matrices:

- $\mathbf{S}^\tau$ For a parent box τ, $\mathbf{S}^\tau$ is a solution operator that maps values of u on $\partial\Omega_\tau$ to values of u at the interior nodes. In other words, $\mathbf{u}(I^\tau_{\text{i}}) = \mathbf{S}^\tau\,\mathbf{u}(I^\tau_{\text{e}})$. (For a leaf τ, $\mathbf{S}^\tau$ is not defined.)
- $\mathbf{T}^\tau$ The matrix that maps $\mathbf{u}(I^\tau_{\text{e}})$ (tabulating values of u on $\partial\Omega_\tau$) to $\mathbf{v}(I^\tau_{\text{e}})$ (tabulating values of du/dn). In other words, $\mathbf{v}(I^\tau_{\text{e}}) = \mathbf{T}^\tau\,\mathbf{u}(I^\tau_{\text{e}})$.

(Recall that the index vector I^τ_{e} and I^τ_{i} were defined in section 2.) The build stage consists of a single sweep over all nodes in the tree. Any bottom-up ordering in which any parent box is processed after its children can be used. For each leaf box τ, an approximation to the local DtN map $\mathbf{T}^\tau$ is constructed using the procedure described in section 3. For a parent box τ with children σ_1 and σ_2, the matrices $\mathbf{S}^\tau$ and $\mathbf{T}^\tau$ are formed from the DtN operators $\mathbf{T}^{\sigma_1}$ and $\mathbf{T}^{\sigma_2}$ via the process described in section 4. Algorithm 1 summarizes the build stage.

Once all the matrices $\{\mathbf{S}^\tau\}_\tau$ have been formed, a vector $\mathbf{u}$ holding approximations to the solution u of (1) can be constructed for all discretization points by starting at the root box Ω and moving down the tree toward the leaf boxes. The values of $\mathbf{u}$ for the points on the boundary of Ω can be obtained by tabulating the boundary function f. When any box τ is processed, the value of $\mathbf{u}$ is known for all nodes on its boundary (i.e., those listed in I^τ_{e}). The matrix $\mathbf{S}^\tau$ directly maps these values to the values of $\mathbf{u}$ on the nodes in the interior of τ (i.e., those listed in I^τ_{i}). When all nodes have been processed, approximations to u have been constructed for all tabulation nodes on interior edges. Algorithm 2 summarizes the solve stage.

Remark 5.1. The merge stage is exact when performed in exact arithmetic. The only approximation involved is the approximation of the solution u on a leaf by its interpolating polynomial.

Remark 5.2. To keep the presentation simple, we consider in this paper only the case of a uniform computational grid. Such grids are obviously not well suited to situations where the regularity of the solution changes across the domain. The method described can *in principle* be modified to handle locally refined grids quite easily.

ALGORITHM 1. BUILD SOLUTION OPERATORS.
This algorithm builds the global Dirichlet-to-Neumann operator for (1).
It also builds all matrices $\mathbf{S}^\tau$ required for constructing u at any interior point.
It is assumed that if node τ is a parent of node σ, then $\tau < \sigma$.

(1) **for** $\tau = N_{\text{boxes}}, N_{\text{boxes}} - 1, N_{\text{boxes}} - 2, \ldots, 1$
(2) **if** (τ is a leaf)
(3) Construct $\mathbf{T}^\tau$ via the process described in section 3.
(4) **else**
(5) Let σ_1 and σ_2 be the children of τ.
(6) Split $I_{\text{e}}^{\sigma_1}$ and $I_{\text{e}}^{\sigma_2}$ into vectors I_1, I_2, and I_3 as shown in Figure 3.
(7) $\mathbf{S}^\tau = \left(\mathbf{T}_{3,3}^{\sigma_1} - \mathbf{T}_{3,3}^{\sigma_2}\right)^{-1} \left[-\mathbf{T}_{3,1}^{\sigma_1} \;\middle|\; \mathbf{T}_{3,2}^{\sigma_2}\right]$
(8) $\mathbf{T}^\tau = \begin{bmatrix} \mathbf{T}_{1,1}^{\sigma_1} & \mathbf{0} \\ \mathbf{0} & \mathbf{T}_{2,2}^{\sigma_2} \end{bmatrix} + \begin{bmatrix} \mathbf{T}_{1,3}^{\sigma_1} \\ \mathbf{T}_{2,3}^{\sigma_2} \end{bmatrix} \mathbf{S}^\tau.$
(9) Delete $\mathbf{T}^{\sigma_1}$ and $\mathbf{T}^{\sigma_2}$.
(10) **end if**
(11) **end for**

ALGORITHM 2. SOLVE BVP ONCE SOLUTION OPERATOR HAS BEEN BUILT.
This program constructs an approximation $\mathbf{u}$ to the solution u of (1).
It assumes that all matrices $\mathbf{S}^\tau$ have already been constructed in a precomputation.
It is assumed that if node τ is a parent of node σ, then $\tau < \sigma$.

(1) $\mathbf{u}(k) = f(\boldsymbol{x}_k)$ for all $k \in I_{\text{e}}^1$.
(2) **for** $\tau = 1, 2, 3, \ldots, N_{\text{boxes}}$
(3) **if** (τ is a parent)
(4) $\mathbf{u}(I_{\text{i}}^\tau) = \mathbf{S}^\tau \, \mathbf{u}(I_{\text{e}}^\tau)$.
(5) **end if**
(6) **end for**
Remark: This algorithm outputs the solution on the Gaussian nodes on box boundaries. To get the solution at other points, use the method described in section 5.3.

A complication is that the tabulation nodes for two touching boxes will typically not coincide, which requires the introduction of specialized interpolation operators. Efficient refinement strategies also require the development of error indicators that identify the regions where the grid needs to be refined. This is work in progress, and will be reported at a later date. We observe that our introduction of Gaussian nodes on the internal boundaries (as opposed to the Chebyshev nodes used in [19]) makes reinterpolation much easier.

5.2. Asymptotic complexity. In this section, we determine the asymptotic complexity of the direct solver. Let $N_{\text{leaf}} = 4q$ denote the number of Gaussian nodes on the boundary of a leaf box, and let q^2 denote the number of Chebyshev nodes used in the leaf computation. Let L denote the number of levels in the binary tree. This means there are 4^L boxes. Thus the total number of discretization nodes N is approximately $4^L q = \frac{(2^L q)^2}{q}$. (To be exact, $N = 2^{2L+1}q + 2^{L+1}q$.)

The cost to process one leaf is approximately $O(q^6)$. Since there are $\frac{N}{q^2}$ leaf boxes, the total cost of precomputing approximate DtN operators for all the bottom level is $\frac{N}{q^2} \times q^6 \sim Nq^4$.

Next, consider the cost of constructing the DtN map on level ℓ via the merge operation described in section 4. For each box on the level ℓ, the operators $\mathbf{T}^\tau$ and $\mathbf{S}^\tau$ are constructed via (14) and (15). These operations involve matrices of size roughly $2^{-\ell}N^{0.5} \times 2^{-\ell}N^{0.5}$. Since there are 4^ℓ boxes per level, the cost on level ℓ of the merge is

$$4^\ell \times \left(2^{-\ell}N^{0.5}\right)^3 \sim 2^{-\ell}N^{1.5}.$$

The total cost for all the merge procedures has complexity

$$\sum_{\ell=1}^{L} 2^{-\ell}N^{1.5} \sim N^{1.5}.$$

Finally, consider the cost of the downwards sweep which solves for the interior unknowns. For any nonleaf box τ on level ℓ, the size of $\mathbf{S}^\tau$ is $2^l q \times 2^l(6q)$ which is approximately $\sim 2^{-\ell}N^{0.5} \times 2^{-\ell}N^{0.5}$. Thus the cost of applying $\mathbf{S}^\tau$ is roughly $(2^{-\ell}N^{0.5})^2 = 2^{-2\ell}N$. So the total cost of the solve step has complexity

$$\sum_{l=0}^{L-1} 2^{2\ell}2^{-2\ell}N \sim N \log N.$$

In section 8, we explain how to exploit structure in the matrices $\mathbf{T}$ and $\mathbf{S}$ to improve the computational cost of both the precomputation and the solve steps.

5.3. Postprocessing. The direct solver in Algorithm 1 constructs approximations to the solution u of (1) at tabulation nodes at all interior edges. Once these are available, it is easy to construct an approximation to u at an arbitrary point. To illustrate the process, suppose that we seek an approximation to $u(\boldsymbol{y})$, where $\boldsymbol{y}$ is a point located in a leaf τ. We have values of u tabulated at Gaussian nodes on $\partial\Omega_\tau$. These can easily be reinterpolated to the Chebyshev nodes on $\partial\Omega_\tau$. Then u can be reconstructed at the interior Chebyshev nodes via the formula (8); observe that the local solution operator $-\mathbf{A}_{\mathrm{i,i}}^{-1}\mathbf{A}_{\mathrm{i,e}}$ was built when the leaf was originally processed and can be simply retrieved from memory (assuming enough memory is available). Once u is tabulated at the Chebyshev grid on Ω_τ, it is trivial to interpolate it to $\boldsymbol{y}$ or any other point.

6. Compressible matrices. The cost of the direct solver given as Algorithm 1 is dominated by the work done at the very top levels; the matrix operations on lines (7) and (8) involve dense matrices of size $O(N^{0.5}) \times O(N^{0.5})$, where N is the total number of discretization nodes, resulting in $O(N^{1.5})$ overall cost. It turns out that these dense matrices have an internal structure that can be exploited to greatly accelerate the matrix algebra. Specifically, the off-diagonal blocks of these matrices are to, high precision, rank deficient, and the matrices can be represented efficiently using a hierarchical "data-sparse" format known as *hierarchically block separable (HBS)* (and sometimes *hierarchically semiseparable (HSS)* matrices [23, 1]). This section briefly describes the HBS property; for details, see [10].

6.1. Block separable. Let $\mathbf{H}$ be an $mp \times mp$ matrix that is blocked into $p \times p$ blocks, each of size $m \times m$. We say that $\mathbf{H}$ is "block separable" with "block-rank" k if for $\tau = 1, 2, \ldots, p$, there exist $m \times k$ matrices $\mathbf{U}_\tau$ and $\mathbf{V}_\tau$ such that each off-diagonal block $\mathbf{H}_{\sigma,\tau}$ of $\mathbf{H}$ admits the factorization

$$\underset{m\times m}{\mathbf{H}_{\sigma,\tau}} = \underset{m\times k}{\mathbf{U}_\sigma}\ \underset{k\times k}{\tilde{\mathbf{H}}_{\sigma,\tau}}\ \underset{k\times m}{\mathbf{V}_\tau^*}, \qquad \sigma,\tau \in \{1, 2, \ldots, p\}, \quad \sigma \neq \tau. \tag{16}$$

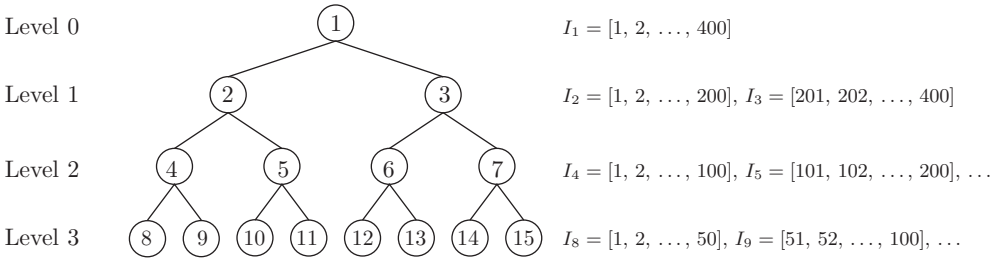

FIG. 4. *Numbering of nodes in a fully populated binary tree with $L = 3$ levels. The root is the original index vector $I = I_1 = [1, 2, \ldots, 400]$.*

Observe that the columns of $\mathbf{U}_\sigma$ must form a basis for the columns of all off-diagonal blocks in row σ and, analogously, the columns of $\mathbf{V}_\tau$ must form a basis for the rows in all the off-diagonal blocks in column τ. When (16) holds, the matrix $\mathbf{H}$ admits a block factorization

$$\underset{mp \times mp}{\mathbf{H}} = \underset{mp \times kp}{\mathbf{U}} \quad \underset{kp \times kp}{\tilde{\mathbf{H}}} \quad \underset{kp \times mp}{\mathbf{V}^*} + \underset{mp \times mp}{\mathbf{D}}, \tag{17}$$

where

$$\mathbf{U} = \operatorname{diag}(\mathbf{U}_1, \mathbf{U}_2, \ldots, \mathbf{U}_p), \quad \mathbf{V} = \operatorname{diag}(\mathbf{V}_1, \mathbf{V}_2, \ldots, \mathbf{V}_p), \quad \mathbf{D} = \operatorname{diag}(\mathbf{D}_1, \mathbf{D}_2, \ldots, \mathbf{D}_p),$$

and

$$\tilde{\mathbf{H}} = \begin{bmatrix} \mathbf{0} & \tilde{\mathbf{H}}_{12} & \tilde{\mathbf{H}}_{13} & \cdots \\ \tilde{\mathbf{H}}_{21} & \mathbf{0} & \tilde{\mathbf{H}}_{23} & \cdots \\ \tilde{\mathbf{H}}_{31} & \tilde{\mathbf{H}}_{32} & \mathbf{0} & \cdots \\ \vdots & \vdots & \vdots & \end{bmatrix}.$$

6.2. Hierarchically block separable. Informally speaking, a matrix $\mathbf{H}$ is hierarchically block separable (HBS), if it is amenable to a *telescoping* block factorization. In other words, in addition to the matrix $\mathbf{H}$ being block separable, so is $\tilde{\mathbf{H}}$ once it has been reblocked to form a matrix with $p/2 \times p/2$ blocks. Likewise, the middle matrix from the block separable factorization of $\tilde{\mathbf{H}}$ will be block separable, etc.

In this section, we describe properties and the factored representation of HBS matrices. Details on constructing the factorization are provided in [10].

6.3. A binary tree structure. The HBS representation of an $M \times M$ matrix $\mathbf{H}$ is based on a partition of the index vector $I = [1, 2, \ldots, M]$ into a binary tree structure. We let I form the root of the tree, and give it the index 1, $I_1 = I$. We next split the root into two roughly equisized vectors I_2 and I_3 so that $I_1 = I_2 \cup I_3$. The full tree is then formed by continuing to subdivide any interval that holds more than some preset fixed number m of indices. We use the integers $\ell = 0, 1, \ldots, L$ to label the different levels, with 0 denoting the coarsest level. A *leaf* is a node corresponding to a vector that never got split. For a nonleaf node τ, its *children* are the two boxes σ_1 and σ_2 such that $I_\tau = I_{\sigma_1} \cup I_{\sigma_2}$, and τ is then the *parent* of σ_1 and σ_2. Two boxes with the same parent are called *siblings*. These definitions are illustrated in Figure 4.

6.4. Definition of the HBS property. We now define what it means for an $M \times M$ matrix $\mathbf{H}$ to be HBS with respect to a given binary tree $\mathcal{T}$ that partitions the

	Name	Size	Function
For each leaf node τ	$\mathbf{D}_\tau$	$m \times m$	The diagonal block $\mathbf{H}(I_\tau, I_\tau)$.
	$\mathbf{U}_\tau$	$m \times k$	Basis for the columns in the blocks in row τ.
	$\mathbf{V}_\tau$	$m \times k$	Basis for the rows in the blocks in column τ.
For each parent node τ	$\mathbf{B}_\tau$	$2k \times 2k$	Interactions between the children of τ.
	$\mathbf{U}_\tau$	$2k \times k$	Basis for the columns in the (reduced) blocks in row τ.
	$\mathbf{V}_\tau$	$2k \times k$	Basis for the rows in the (reduced) blocks in column τ.

FIG. 5. *An HBS matrix* $\mathbf{H}$ *associated with a tree* $\mathcal{T}$ *is fully specified if the factors listed above are provided.*

index vector $J = [1, 2, \ldots, M]$. For simplicity, we suppose that for every leaf node τ the index vector I_τ holds precisely m points, so that $M = m\,2^L$. Then $\mathbf{H}$ is HBS with block rank k if the following two conditions hold.

(1) *Assumption on ranks of off-diagonal blocks at the finest level:* For any two distinct leaf nodes τ and τ', define the $m \times m$ matrix

$$\mathbf{H}_{\tau,\tau'} = \mathbf{H}(I_\tau, I_{\tau'}). \tag{18}$$

Then there must exist matrices $\mathbf{U}_\tau$, $\mathbf{V}_{\tau'}$, and $\tilde{\mathbf{H}}_{\tau,\tau'}$ such that

$$\begin{array}{ccccc} \mathbf{H}_{\tau,\tau'} & = & \mathbf{U}_\tau & \tilde{\mathbf{H}}_{\tau,\tau'} & \mathbf{V}^*_{\tau'}. \\ m \times m & & m \times k & k \times k & k \times m \end{array} \tag{19}$$

(2) *Assumption on ranks of off-diagonal blocks on level* $\ell = L-1, L-2, \ldots, 1$*:* The rank assumption at level ℓ is defined in terms of the blocks constructed on the next finer level $\ell + 1$. For any distinct nodes τ and τ' on level ℓ with children σ_1, σ_2 and σ'_1, σ'_2, respectively, define

$$\mathbf{H}_{\tau,\tau'} = \begin{bmatrix} \tilde{\mathbf{H}}_{\sigma_1,\sigma'_1} & \tilde{\mathbf{H}}_{\sigma_1,\sigma'_2} \\ \tilde{\mathbf{H}}_{\sigma_2,\sigma'_1} & \tilde{\mathbf{H}}_{\sigma_2,\sigma'_2} \end{bmatrix}. \tag{20}$$

Then there must exist matrices $\mathbf{U}_\tau$, $\mathbf{V}_{\tau'}$, and $\tilde{\mathbf{H}}_{\tau,\tau'}$ such that

$$\begin{array}{ccccc} \mathbf{H}_{\tau,\tau'} & = & \mathbf{U}_\tau & \tilde{\mathbf{H}}_{\tau,\tau'} & \mathbf{V}^*_{\tau'}. \\ 2k \times 2k & & 2k \times k & k \times k & k \times 2k \end{array} \tag{21}$$

An HBS matrix is now fully described if the basis matrices $\mathbf{U}_\tau$ and $\mathbf{V}_\tau$ are provided for each node τ, and in addition, we are, for each leaf τ, given the $m \times m$ matrix

$$\mathbf{D}_\tau = \mathbf{H}(I_\tau, I_\tau), \tag{22}$$

and for each parent node τ with children σ_1 and σ_2 we are given the $2k \times 2k$ matrix

$$\mathbf{B}_\tau = \begin{bmatrix} 0 & \tilde{\mathbf{H}}_{\sigma_1,\sigma_2} \\ \tilde{\mathbf{H}}_{\sigma_2,\sigma_1} & 0 \end{bmatrix}. \tag{23}$$

Observe in particular that the matrices $\tilde{\mathbf{H}}_{\sigma_1,\sigma_2}$ are only required when $\{\sigma_1, \sigma_2\}$ forms a sibling pair. Figure 5 summarizes the required matrices.

6.5. Telescoping factorization. Given the matrices defined in the previous section, we define the following block diagonal factors:

$$\underline{\mathbf{D}}^{(\ell)} = \operatorname{diag}(\mathbf{D}_\tau : \tau \text{ is a box on level } \ell), \qquad \ell = 0, 1, \ldots, L, \tag{24}$$

$$\underline{\mathbf{U}}^{(\ell)} = \operatorname{diag}(\mathbf{U}_\tau : \tau \text{ is a box on level } \ell), \qquad \ell = 1, 2, \ldots, L, \tag{25}$$

$$\underline{\mathbf{V}}^{(\ell)} = \operatorname{diag}(\mathbf{V}_\tau : \tau \text{ is a box on level } \ell), \qquad \ell = 1, 2, \ldots, L, \tag{26}$$

$$\underline{\mathbf{B}}^{(\ell)} = \operatorname{diag}(\mathbf{B}_\tau : \tau \text{ is a box on level } \ell), \qquad \ell = 0, 1, \ldots, L-1. \tag{27}$$

Furthermore, we let $\tilde{\mathbf{H}}^{(\ell)}$ denote the block matrix whose diagonal blocks are zero, and whose off-diagonal blocks are the blocks $\tilde{\mathbf{H}}_{\tau,\tau'}$ for all distinct τ, τ' on level ℓ. With these definitions,

$$\underset{m\,2^L \times n\,2^L}{\mathbf{H}} = \underset{m\,2^L \times k\,2^L}{\underline{\mathbf{U}}^{(L)}} \quad \underset{k\,2^L \times k\,2^L}{\tilde{\mathbf{H}}^{(L)}} \quad \underset{k\,2^L \times m\,2^L}{(\underline{\mathbf{V}}^{(L)})^*} + \underset{m\,2^L \times m\,2^L}{\underline{\mathbf{D}}^{(L)}}; \tag{28}$$

for $\ell = L-1,\, L-2, \ldots, 1$ we have

$$\underset{k\,2^{\ell+1} \times k\,2^{\ell+1}}{\tilde{\mathbf{H}}^{(\ell+1)}} = \underset{k\,2^{\ell+1} \times k\,2^{\ell}}{\underline{\mathbf{U}}^{(\ell)}} \quad \underset{k\,2^{\ell} \times k\,2^{\ell}}{\tilde{\mathbf{H}}^{(\ell)}} \quad \underset{k\,2^{\ell} \times k\,2^{\ell+1}}{(\underline{\mathbf{V}}^{(\ell)})^*} + \underset{k\,2^{\ell+1} \times k\,2^{\ell+1}}{\underline{\mathbf{B}}^{(\ell)}}; \tag{29}$$

and finally

$$\tilde{\mathbf{H}}^{(1)} = \underline{\mathbf{B}}^{(0)}. \tag{30}$$

7. Fast arithmetic operations on HBS matrices. Arithmetic operations involving dense HBS matrices of size $M \times M$ can often be executed in $O(M)$ operations. This fast matrix algebra is vital for achieving linear complexity in our direct solver. This section provides a brief introduction to the HBS matrix algebra. We describe the operations we need (inversion, addition, and low-rank update) in some detail for the single level "block separable" format. The generalization to the multilevel HBS format is briefly described for the case of matrix inversion. A full description of all algorithms required is given in [8], which is related to the earlier work [2].

Before we start, we recall that a block separable matrix $\mathbf{H}$ consisting of $p \times p$ blocks, each of size $m \times m$, and with "HBS rank" $k < m$, admits the factorization

$$\underset{mp \times mp}{\mathbf{H}} = \underset{mp \times kp}{\mathbf{U}} \quad \underset{kp \times kp}{\tilde{\mathbf{H}}} \quad \underset{kp \times mp}{\mathbf{V}^*} + \underset{mp \times mp}{\mathbf{D}}. \tag{31}$$

7.1. Inversion of a block separable matrix. The decomposition (31) represents $\mathbf{H}$ as a sum of one term $\mathbf{U}\tilde{\mathbf{H}}\mathbf{V}^*$ that is "low rank," and one term $\mathbf{D}$ that is easily invertible (since it is block diagonal). By modifying the classical Woodbury formula for inversion of a matrix perturbed by the addition of a low-rank term, it can be shown that (see Lemma 3.1 of [10])

$$\mathbf{H}^{-1} = \mathbf{E}\,(\tilde{\mathbf{H}} + \hat{\mathbf{D}})^{-1}\,\mathbf{F}^* + \mathbf{G}, \tag{32}$$

where

$$\hat{\mathbf{D}} = \left(\mathbf{V}^*\,\mathbf{D}^{-1}\,\mathbf{U}\right)^{-1}, \tag{33}$$

$$\mathbf{E} = \mathbf{D}^{-1}\,\mathbf{U}\,\hat{\mathbf{D}}, \tag{34}$$

$$\mathbf{F} = (\hat{\mathbf{D}}\,\mathbf{V}^*\,\mathbf{D}^{-1})^*, \tag{35}$$

$$\mathbf{G} = \mathbf{D}^{-1} - \mathbf{D}^{-1}\,\mathbf{U}\,\hat{\mathbf{D}}\,\mathbf{V}^*\,\mathbf{D}^{-1}, \tag{36}$$

assuming the inverses in formulas (32)–(36) all exist. Now observe that the matrices

$\hat{\mathbf{D}}$, $\mathbf{E}$, $\mathbf{F}$, and $\mathbf{G}$ can all easily be computed since the formulas defining them involve only block-diagonal matrices. In consequence, (32) reduces the task of inverting the big (size $mp \times mp$) matrix $\mathbf{H}$ to the task of inverting the small (size $kp \times kp$) matrix $\tilde{\mathbf{H}} + \hat{\mathbf{D}}$.

When $\mathbf{H}$ is not only "block separable," but HBS, the process can be repeated recursively by exploiting that $\tilde{\mathbf{H}} + \hat{\mathbf{D}}$ is itself amenable to accelerated inversion, etc. The resulting process is somewhat tricky to analyze, but leads to very clean codes. To illustrate, we include Algorithm 3 which shows the multilevel $O(M)$ inversion algorithm for an HBS matrix $\mathbf{H}$. The algorithm takes as input the factors $\{\mathbf{U}_\tau, \mathbf{V}_\tau, \mathbf{D}_\tau, \mathbf{B}_\tau\}_\tau$ representing $\mathbf{H}$ (cf. Figure 5), and outputs an analogous set of factors $\{\mathbf{E}_\tau, \mathbf{F}_\tau, \mathbf{G}_\tau\}_\tau$ representing $\mathbf{H}^{-1}$. With these factors, the matrix-vector multiplication $\mathbf{y} = \mathbf{H}^{-1}\mathbf{x}$ can be executed via the procedure described in Algorithm 4.

ALGORITHM 3. INVERSION OF AN HBS MATRIX.

Given factors $\{\mathbf{U}_\tau, \mathbf{V}_\tau, \mathbf{D}_\tau, \mathbf{B}_\tau\}_\tau$ representing an HBS matrix $\mathbf{H}$, this algorithm constructs factors $\{\mathbf{E}_\tau, \mathbf{F}_\tau, \mathbf{G}_\tau\}_\tau$ representing $\mathbf{H}^{-1}$.

loop over all levels, finer to coarser, $\ell = L, L-1, \ldots, 1$
  loop over all boxes τ on level ℓ,
    if τ is a leaf node
      $\tilde{\mathbf{D}}_\tau = \mathbf{D}_\tau$
    else
      Let σ_1 and σ_2 denote the children of τ.
      $\tilde{\mathbf{D}}_\tau = \begin{bmatrix} \hat{\mathbf{D}}_{\sigma_1} & \mathbf{B}_{\sigma_1,\sigma_2} \\ \mathbf{B}_{\sigma_2,\sigma_1} & \hat{\mathbf{D}}_{\sigma_2} \end{bmatrix}$
    end if
    $\hat{\mathbf{D}}_\tau = \left(\mathbf{V}_\tau^* \tilde{\mathbf{D}}_\tau^{-1} \mathbf{U}_\tau\right)^{-1}$.
    $\mathbf{E}_\tau = \tilde{\mathbf{D}}_\tau^{-1} \mathbf{U}_\tau \hat{\mathbf{D}}_\tau$.
    $\mathbf{F}_\tau^* = \hat{\mathbf{D}}_\tau \mathbf{V}_\tau^* \tilde{\mathbf{D}}_\tau^{-1}$.
    $\mathbf{G}_\tau = \tilde{\mathbf{D}}_\tau^{-1} - \tilde{\mathbf{D}}_\tau^{-1} \mathbf{U}_\tau \hat{\mathbf{D}}_\tau \mathbf{V}_\tau^* \tilde{\mathbf{D}}_\tau^{-1}$.
  end loop
end loop
$\mathbf{G}_1 = \begin{bmatrix} \hat{\mathbf{D}}_2 & \mathbf{B}_{2,3} \\ \mathbf{B}_{3,2} & \hat{\mathbf{D}}_3 \end{bmatrix}^{-1}$.

7.2. Addition of two block separable matrices. Let $\mathbf{H}^A$ and $\mathbf{H}^B$ be block separable matrices with factorizations

$$\mathbf{H}^A = \mathbf{U}^A \tilde{\mathbf{H}}^A \mathbf{V}^{A*} + \mathbf{D}^A, \qquad \text{and} \qquad \mathbf{H}^B = \mathbf{U}^B \tilde{\mathbf{H}}^B \mathbf{V}^{B*} + \mathbf{D}^B.$$

Then $\mathbf{H} = \mathbf{H}^A + \mathbf{H}^B$ can be written in block separable form via

$$\mathbf{H} = \mathbf{H}^A + \mathbf{H}^B = \begin{bmatrix} \mathbf{U}^A \, \mathbf{U}^B \end{bmatrix} \begin{bmatrix} \tilde{\mathbf{H}}^A & 0 \\ 0 & \tilde{\mathbf{H}}^B \end{bmatrix} \begin{bmatrix} \mathbf{V}^A \, \mathbf{V}^B \end{bmatrix}^* + \left(\mathbf{D}^A + \mathbf{D}^B\right). \tag{37}$$

To restore (37) to block separable form, permute the rows and columns of $[\mathbf{U}^A \, \mathbf{U}^B]$ and $[\mathbf{V}^A \, \mathbf{V}^B]$ to attain block diagonal form, then reorthogonalize the diagonal blocks. This process in principle results in a matrix $\mathbf{H}$ whose HBS rank is the sum of the HBS ranks of $\mathbf{H}^A$ and $\mathbf{H}^B$. In practice, this rank increase can be combated by numerically recompressing the basis matrices, and updating the middle factor as needed. For details, as well as the extension to a multilevel scheme, see [2, 8].

ALGORITHM 4. APPLICATION OF THE INVERSE OF AN HBS MATRIX.
Given $\mathbf{x}$*, compute* $\mathbf{y} = \mathbf{H}^{-1}\mathbf{x}$ *using the factors* $\{\mathbf{E}_\tau, \mathbf{F}_\tau, \mathbf{G}_\tau\}_\tau$ *resulting from Algorithm* 3.

loop over all leaf boxes τ
  $\hat{\mathbf{x}}_\tau = \mathbf{F}_\tau^* \mathbf{x}(I_\tau)$.
end loop

loop over all levels, finer to coarser, $\ell = L, L-1, \ldots, 1$
  loop over all parent boxes τ on level ℓ,
    Let σ_1 and σ_2 denote the children of τ.
    $\hat{\mathbf{x}}_\tau = \mathbf{F}_\tau^* \begin{bmatrix} \hat{\mathbf{x}}_{\sigma_1} \\ \hat{\mathbf{x}}_{\sigma_2} \end{bmatrix}$.
  end loop
end loop

$\begin{bmatrix} \hat{\mathbf{y}}_2 \\ \hat{\mathbf{y}}_3 \end{bmatrix} = \mathbf{G}_1 \begin{bmatrix} \hat{\mathbf{x}}_2 \\ \hat{\mathbf{x}}_3 \end{bmatrix}$.

loop over all levels, coarser to finer, $\ell = 1, 2, \ldots, L-1$
  loop over all parent boxes τ on level ℓ
    Let σ_1 and σ_2 denote the children of τ.
    $\begin{bmatrix} \hat{\mathbf{y}}_{\sigma_1} \\ \hat{\mathbf{y}}_{\sigma_2} \end{bmatrix} = \mathbf{E}_\tau \hat{\mathbf{x}}_\tau + \mathbf{G}_\tau \begin{bmatrix} \hat{\mathbf{x}}_{\sigma_1} \\ \hat{\mathbf{x}}_{\sigma_2} \end{bmatrix}$.
  end loop
end loop

loop over all leaf boxes τ
  $\mathbf{y}(I_\tau) = \mathbf{E}_\tau \hat{\mathbf{q}}_\tau + \mathbf{G}_\tau \mathbf{x}(I_\tau)$.
end loop

7.3. Addition of a block separable matrix with a low rank matrix. Let $\mathbf{H}^B = \mathbf{QR}$ be a k-rank matrix where $\mathbf{Q}$ and $\mathbf{R}^*$ are of size $mp \times k$. We would like to add $\mathbf{H}^B$ to the block separable matrix $\mathbf{H}^A$. Since we already know how to add two block separable matrices, we choose to rewrite $\mathbf{H}^B$ in block separable form. Without loss of generality, assume $\mathbf{Q}$ is orthogonal. Partition $\mathbf{Q}$ into p blocks of size $m \times k$. The blocks make up the matrix $\mathbf{U}^B$. Likewise partition $\mathbf{R}$ into p blocks of size $k \times m$. The block matrix $\mathbf{D}^B$ has entries $\mathbf{D}_\tau = \mathbf{Q}_\tau \mathbf{R}_\tau$ for $\tau = 1, \ldots, p$. To construct the matrices $\mathbf{V}^B$, for each $\tau = 1, \ldots, p$, the matrix $\mathbf{R}_\tau$ is factorized into $\tilde{\mathbf{R}}_\tau \mathbf{V}_\tau *$ where the matrix $\mathbf{V}_\tau$ is orthogonal. The matrices $\tilde{\mathbf{R}}_\tau$ make up the entries of $\tilde{\mathbf{H}}^B$.

8. Accelerating the direct solver. This section describes how the fast matrix algebra described in sections 6 and 7 can be used to accelerate the direct solver of section 5 to attain $O(N)$ complexity. We recall that the $O(N^{1.5})$ cost of Algorithm 1 relates to the execution of lines (7) and (8) at the top levels, since these involve dense matrix algebra of matrices of size $O(N^{0.5}) \times O(N^{0.5})$. The principal claims of this section are

- the matrices $\mathbf{T}_{1,3}^{\sigma_1}$, $\mathbf{T}_{3,1}^{\sigma_1}$; $\mathbf{T}_{2,3}^{\sigma_2}$, $\mathbf{T}_{3,2}^{\sigma_2}$. have low numerical rank;
- the matrices $\mathbf{T}_{1,1}^{\sigma_1}$, $\mathbf{T}_{2,2}^{\sigma_2}$, $\mathbf{T}_{3,3}^{\sigma_1}$, $\mathbf{T}_{3,3}^{\sigma_2}$ are HBS matrices of low HBS rank.

To be precise, the ranks that we claim are "low" scale as $\log(1/\nu) \times \log(m)$, where m is the number of points along the boundary of Ω_τ, and ν is the computational tolerance. In practice, we found that for problems with nonoscillatory solutions, the ranks are extremely modest: When $\nu = 10^{-10}$, the ranks range between 10 and 80, even for very large problems.

The cause of the rank deficiencies is that the matrix $\mathbf{T}^\tau$ is a highly accurate approximation to the DtN operator on Ω_τ. This operator is known to have a smooth kernel that is nonoscillatory whenever the underlying PDE has nonoscillatory solutions. Since the domain boundary $\partial\Omega_\tau$ is one dimensional, this makes the expectation that the off-diagonal blocks have low rank very natural; see [10]. It is backed up by extensive numerical experiments (see section 9), but we do not at this point have rigorous proofs to support the claim.

Once it is observed that all matrices in lines (7) and (8) of Algorithm 1 are structured, it becomes obvious how to accelerate the algorithm. For instance, line (7) is executed in three steps: (i) Add the HBS matrices $\mathbf{T}^{\sigma_1}_{3,3}$ and $-\mathbf{T}^{\sigma_2}_{3,3}$; (ii) invert the sum of the HBS matrices; (iii) apply the inverse (in HBS form) to one of the low-rank factors of $\big[-\mathbf{T}^{\alpha}_{3,1} \;\big|\; \mathbf{T}^{\beta}_{3,2}\big]$. The result is an approximation to $\mathbf{S}^\tau$, represented as a product of two thin matrices. Executing line (8) is analogous: First form the matrix products $\mathbf{T}^{\sigma_1}_{1,3}\,\mathbf{S}^\tau$ and $\mathbf{T}^{\sigma_2}_{2,3}\,\mathbf{S}^\tau$, exploiting that all factors are of low rank. Then perform a low-rank update to a block-diagonal matrix whose blocks are provided in HBS-form to construct the new HBS matrix $\mathbf{T}^\tau$.

Accelerating the solve stage in Algorithm 2 is trivial, simply exploit that the matrix $\mathbf{S}^\tau$ on line (3) has low numerical rank.

Remark 8.1. Some of the structured matrix operators (e.g., adding two HBS matrices, or the low-rank update) can algebraically lead to a large increase in the HBS ranks. We know for physical reasons that the output should have rank structure very similar to the input, however, and we combat the rank increase by frequently recompressing the output of each operation.

Remark 8.2. In practice, we implement the algorithm to use dense matrix algebra at the finer levels, where all the DtN matrices $\mathbf{T}^\tau$ are small. Once they get large enough that HBS algebra outperforms dense operations, we compress the dense matrices by brute force, and rely on HBS algebra in the remainder of the upwards sweep.

9. Numerical examples. In this section, we illustrate the capabilities of the proposed method for the boundary value problem

$$\begin{cases} -\Delta u(\boldsymbol{x}) - c_1(\boldsymbol{x})\,\partial_1 u(\boldsymbol{x}) - c_2(\boldsymbol{x})\,\partial_2 u(\boldsymbol{x}) - c(\boldsymbol{x})\,u(\boldsymbol{x}) = 0, & \boldsymbol{x} \in \Omega, \\ u(\boldsymbol{x}) = f(\boldsymbol{x}), & \boldsymbol{x} \in \Gamma, \end{cases} \tag{38}$$

where $\Omega = [0,1]^2$, $\Gamma = \partial\Omega$, and $c_1(\boldsymbol{x})$, $c_2(\boldsymbol{x})$, and $c(\boldsymbol{x})$ are smooth; cf. (2). The choice of the functions $c_1(\boldsymbol{x})$, $c_2(\boldsymbol{x})$, and $c(\boldsymbol{x})$ will vary for each example.

All experiments reported in this section were executed on a machine with two quad-core 3.3 GHz Intel Xeon E5-2643 processors and 128 GB of RAM. The direct solver was implemented in MATLAB, which means that the speeds reported can very likely be improved, although the asymptotic complexity should be unaffected.

In section 9.1 we apply the direct solver to four problems with known analytic solutions. This allows us to very accurately investigate the errors incurred, but is arguably a particularly favorable environment. Section 9.2 presents results from more general situations where the exact solution is not known, and errors have to be estimated.

In all experiments, the number of Gaussian points per leaf edge q is fixed at 21, and 21×21 tensor product grids of Chebyshev points are used in the leaf computations. Per Remark 8.2, we switch from dense computations to HBS when a box has more than 2000 points on the boundary.

TABLE 1

Timing results in seconds for the PDEs considered in section 9.1. *For these experiments,* $\epsilon = 10^{-7}$. *Note that memory requirements grow as the wave number grows, which is why we could handle* $N = 115909633$ *only for Laplace and Helmholtz I.*

	N_{tot}	N	T_{build} (seconds)	T_{solve} (seconds)	T_{apply} (seconds)	R (MB)	E_{pot}
Laplace	1815681	174720	91.68	0.34	0.035	1611.19	1.41e-04
	7252225	693504	371.15	1.803	0.104	6557.27	3.57e-4
	28987905	2763264	1661.97	6.97	0.168	26503.29	1.23e-3
	115909633	11031552	6894.31	30.67	0.367	106731.61	4.70e-3
Helmholtz I	1815681	174720	62.07	0.202	0.027	1611.41	1.10e-4
	7252225	693504	363.19	1.755	0.084	6557.12	1.19e-4
	28987905	2763264	1677.92	6.92	0.186	26503.41	2.48e-4
	115909633	11031552	7584.65	31.85	0.435	106738.85	2.3e-3
Helmholtz II	1815681	174720	93.96	0.29	0.039	1827.72	1.62e-05
	7252225	693504	525.92	2.13	0.074	7151.60	2.89e-05
	28987905	2763264	2033.91	8.59	0.175	27985.41	1.82e-04
Helmholtz III	1815681	174720	93.68	0.29	0.038	1839.71	5.03e-05
	7252225	693504	624.24	1.67	0.086	7865.13	6.76e-05
	28987905	2763264	4174.91	10.28	0.206	33366.45	1.78e-04

9.1. Performance for problems with known solutions. To illustrate the scaling and accuracy of the discretization technique, we apply the numerical method to four problems with known solutions. The problems are as follows.

Laplace: Let $c_1(\boldsymbol{x}) = c_2(\boldsymbol{x}) = c(\boldsymbol{x}) = 0$ in (38).

Helmholtz I: Let $c_1(\boldsymbol{x}) = c_2(\boldsymbol{x}) = 0$, and $c(\boldsymbol{x}) = \kappa^2$, where $\kappa = 80$ in (38). This represents a vibration problem on a domain Ω of size roughly 12×12 wavelengths. (Recall that the wavelength is given by $\lambda = \frac{2\pi}{\kappa}$.)

Helmholtz II: Let $c_1(\boldsymbol{x}) = c_2(\boldsymbol{x}) = 0$, and $c(\boldsymbol{x}) = \kappa^2$, where $\kappa = 640$ in (38). This corresponds to a domain of size roughly 102×102 wavelengths.

Helmholtz III: We again set $c_1(\boldsymbol{x}) = c_2(\boldsymbol{x}) = 0$, and $c(\boldsymbol{x}) = \kappa^2$ in (38), but now we let κ grow as the number of discretization points grows to maintain a constant 12 points per wavelength.

The boundary data in (38) are chosen to coincide with the known solutions $u_{\text{exact}}(\boldsymbol{x}) = \log|\hat{\boldsymbol{x}} - \boldsymbol{x}|$ for the Laplace problem and with $u_{\text{exact}}(\boldsymbol{x}) = \mathrm{Y}_0(\kappa|\hat{\boldsymbol{x}} - \boldsymbol{x}|)$ for the three Helmholtz problems, where $\hat{\boldsymbol{x}} = (-2, 0)$, and where Y_0 denotes the zeroth Bessel function of the second kind.

In a first experiment, we prescribed the tolerance in the "fast" matrix algebra to be $\epsilon = 10^{-7}$. Table 1 reports the following quantities:

- N Number of Gaussian discretization points.
- N_{tot} Total number of discretization points (N plus the number of Chebyshev points).
- T_{build} Time for building the solution operator.
- T_{solve} Time to solve for interior nodes (edge nodes only) once solution operator is built.
- T_{apply} Time to apply the approximate DtN operator $\mathbf{T}^1$.
- R Amount of memory required to store the solution operator.

In addition, Table 1 reports the relative error in the computed solution u_{app} via the measure

$$E_{\text{pot}} = \frac{\max\left\{\left|u_{\text{app}}(\boldsymbol{x}_k) - u_{\text{exact}}(\boldsymbol{x}_k)\right|\right\}_{k=1}^{N}}{\max\left\{\left|u_{\text{exact}}(\boldsymbol{x}_k)\right|\right\}_{k=1}^{N}},$$

where $\{\boldsymbol{x}_k\}_k$ are the Gaussian nodes on all internal boundaries.

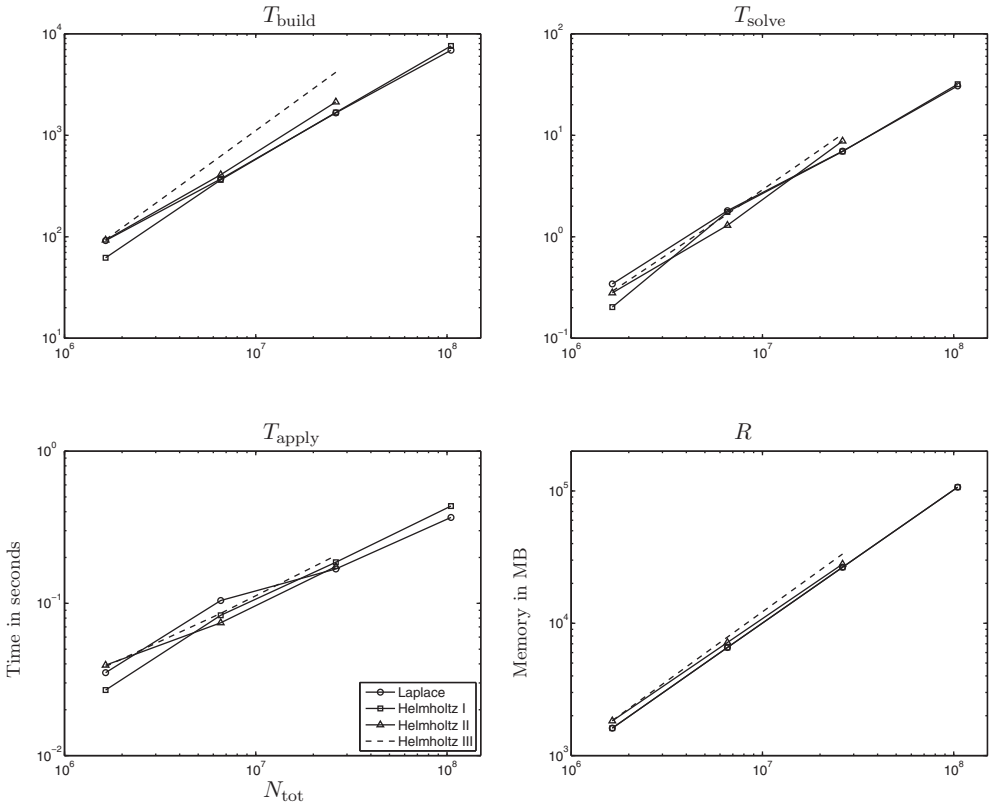

FIG. 6. *The first three graphs give the times required for building the direct solver* (T_{build}), *solving a problem* (T_{solve}), *and applying the approximate DtN operator on* $\partial\Omega$(T_{apply}). *The fourth graph gives the memory* R *in MB required to store the solution operator.*

Our expectation is for all problems except Helmholtz III to exhibit optimal linear scaling for both the build and the solve stages. Additionally, we expect the cost of applying the DtN operator $\mathbf{T}^1$ to scale as $N^{0.5}$ for all problems except Helmholtz III. The numerical results clearly bear this out for Laplace and Helmholtz I. For Helmholtz II, it appears that linear scaling has not quite taken hold for the range of problem sizes our hardware could manage. The Helmholtz III problem clearly does not exhibit linear scaling, but has not yet reached its $O(N^{1.5})$ asymptote at the largest problem considered, which was of size roughly 426×426 wavelengths. We see that the cost of the solve stage is tiny. For example, a problem involving 11 million unknowns (corresponding to approximately 100 million discretization points) takes 115 minutes for the build stage and then only 30 seconds for each additional solve. The cost for applying the DtN operator is even less at 0.36 seconds per boundary condition. Figure 6 illustrates the scaling via log-log plots.

Remark 9.1. It may at first seem counterintuitive that the errors E_{pot} reported in Table 1 increase as N grows, but this is explained by the fact that E_{pot} is a combined error metric that encapsulates both discretization errors and solver errors. While the discretization errors decrease as N increases when the problem is held fixed (as in Laplace I, and in Helmholtz I and II), the solver errors tend to slowly increase, due to aggregation of truncation errors as the number of levels increase. In Table 1, the solver errors tend to dominate, which explains why the errors increase as N grows (this

TABLE 2

Convergence results for solving the PDE's in section 9.2 *with a user prescribed tolerance of* $\epsilon = 10^{-12}$.

	N_{tot}	N	$u^N(\hat{\boldsymbol{x}})$	E^N_{int}	$u^N_n(\hat{\boldsymbol{x}})$	E^N_{bnd}
Constant convection	455233	44352	−0.474057246846306	0.477	−192794.835134257	824.14
	1815681	174720	−0.951426960146812	8.28e-03	−191970.688228300	1.47
	7252225	693504	−0.959709514830931	6.75e-10	−191972.166912008	0.365
	28987905	2763264	−0.959709515505929		−191972.532606428	
Variable Helmholtz	114465	11424	2.50679456864385	6.10e-02	−2779.09822864819	3188
	455233	44352	2.56780367343056	4.63e-07	409.387483435691	2.59e-02
	1815681	174720	2.56734097240752	1.77e-09	409.413356177218	3.30e-07
	7252225	693504	2.56734097418159		409.413355846946	
Diffusion convection	455233	44352	0.0822281612709325	5.04e-5	−35.1309711271060	2.23e-3
	1815681	174720	0.0822785917678385	2.67e-8	−35.1332056731696	7.57e-6
	7252225	693504	0.0822786184699243	5.41e-12	−35.1332132455725	2.11e-09
	28987905	2763264	0.0822786184753420		−35.1332132476795	

TABLE 3

Time and memory requirements for LU-factorization of cross-shaped finite difference stencils on a regular grid in the plane using UMFPACK.

Matrix	N	T_{build} (seconds)	T_{solve} (seconds)	R (MB)	E_{pot} Helm-I	E_{pot} Helm-II	E_{pot} Helm-III
5-point stencil	40000	2.46e-1	5.32e-3	38.26	2.7e0	1.2e0	3.1e0
$O(h^2)$	160000	1.29	2.74e-2	211.43	2.0e1	2.5e1	1.9e1
	640000	6.87	1.33e-1	1073.39	3.1e-1	6.7e1	1.4e1
	2560000	49.86	6.98e-1	5959.00	6.1e-2	8.8e1	3.7e1
	10240000	277.31	3.134	27588.61	1.5e-2	1.6e1	3.5e1
9-point stencil	40000	6.78e-1	1.42e-2	123.82	≥5.5e-2	≥3.8e0	≥1.3e0
$O(h^4)$	160000	4.18	7.59e-2	726.62	≥8.0e-3	≥1.8e1	≥3.2e-1
	640000	35.83	3.80e-1	3509.28	≥1.4e-4	≥1.4e1	≥9.6e-1
	2560000	383.04	2.12	18817.29	≥1.0e-5	≥6.1e-1	≥2.4e0
13-point stencil	40000	1.51	2.81e-2	285.08	≥4.7e-4	≥8.7e1	≥8.6e-3
$O(h^6)$	160000	9.76	1.59e-1	1575.29	≥1.7e-5	≥1.1e1	≥1.3e-1
	640000	164.33	9.03e-1	86661.39	≥5.9e-7	≥4.9e-1	≥2.9e-1
	2560000	1581.11	5.19	42191.17	≥4.1e-9	≥8.3e-2	≥1.4e-1

behavior is in contrast to Table 2, where the solver error is small and discretization errors dominate).

To provide a reference for the computational times and errors reported in Table 1 for our $O(N)$ solver, we give in Table 3 the build and solve times, and errors, for a classical $O(N^{3/2})$ multifrontal solver, as implemented in UMFPACK [5] (using the MATLAB "`lu`" command); cf. Figure 7. We used UMFPACK to compute LU-factorizations of finite difference matrices discretizing a convection-diffusion problem on a regular square grid using three different stencils: The classical 5-point stencil with $O(h^2)$ accuracy, and the cross-shaped 9-point and 13-point stencils with accuracies $O(h^4)$ and $O(h^6)$, respectively. For the cross-shaped 9-point and 13-point stencils, the errors reported are lower bounds only (to ensure that we made the comparison as favorable to finite difference methods as possible, we cheated and provided the solver with the exact solution not only on the boundary, but on one or two layers inside the domain as well). Some observations: (1) The performance of the multifrontal method deteriorates rapidly as the order of the discretization is increased (note that even the 13-point stencil is a low-order method when compared to the proposed scheme); (2) the multifrontal method ran out of memory much earlier than our $O(N)$ method, in particular, for the high-order stencils; (3) the break-even points between our $O(N)$

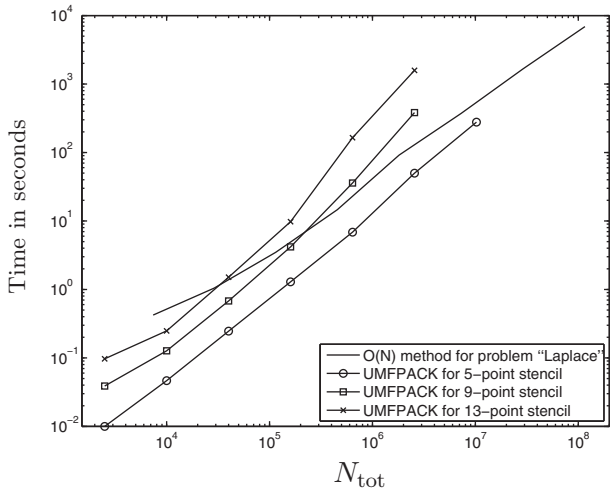

FIG. 7. *Comparison between T_{build} for the proposed method (applied to problem "Laplace" with truncation error $\varepsilon = 10^{-7}$) and UMFPACK applied to the linear systems arising from cross-shaped* 5-, 9-, *and* 13-*point stencils.*

TABLE 4

Errors for solving the PDEs in section 9.1 *with different user prescribed tolerances when the number of discretization points is fixed at $N = 693504$ ($N_{\text{tot}} = 7252225$).*

	$\epsilon = 10^{-7}$		$\epsilon = 10^{-10}$		$\epsilon = 10^{-12}$	
	E_{pot}	E_{grad}	E_{pot}	E_{grad}	E_{pot}	E_{grad}
Laplace	3.57e-04	1.35e-02	1.59e-07	6.92e-06	7.32e-10	1.01e-07
Helmholtz I	1.19e-04	1.31e-04	7.99e-08	9.72e-08	2.06e-09	1.71e-09
Helmholtz II	2.90e-05	2.19e-05	5.72e-08	5.02e-08	6.21e-09	4.64e-09
Helmholtz III	6.76e-05	5.05e-05	1.21e-07	1.31e-07	1.05e-07	1.10e-07

scheme and UMFPACK is quite high for the very low-order 5-point stencil (about $N = 25 \cdot 10^6$), but is very low for the 9- and 13-point stencils ($N = 2.5 \cdot 10^5$ and $N = 3.2 \cdot 10^4$, respectively); (4) the discretization errors resulting from finite difference discretizations are very large, even for relatively high order methods such as the $O(h^6)$ order accurate 13-point stencil.

In a second set of experiments, we investigated the accuracy of the computed solutions, and in particular how the accuracy depends on the tolerance ϵ in the fast matrix algebra. In addition to reporting E_{pot}, Table 4 reports

$$E_{\text{grad}} = \frac{\max_{k:\, \boldsymbol{x}_k \in \Gamma} \left\{ \left| u_{n,\text{app}}(\boldsymbol{x}_k) - u_{n,\text{exact}}(\boldsymbol{x}_k) \right| \right\}}{\max_{k:\, \boldsymbol{x}_k \in \Gamma} \left\{ \left| u_{n,\text{exact}}(\boldsymbol{x}_k) \right| \right\}},$$

where $u_{n,\text{app}}$ denotes the approximate normal derivative of the solution constructed by the direct solver for tolerances $\varepsilon = 10^{-7}$, 10^{-10}, and 10^{-12} and $u_{n,\text{exact}}$ denotes the normal derivative of the solution. The number of edge nodes was fixed at $N = 693504$ ($N_{\text{tot}} = 7252225$).

The solution obtains (or nearly obtains) the prescribed tolerance while the normal derivative suffers from about a three digit loss in accuracy. This loss is likely attributable to the unboundedness of the DtN map. The compressed representation captures the high end of the spectrum to the desired accuracy while the low end of the spectrum is captured to three digits less than the desired accuracy.

TABLE 5
Times in seconds for solving the PDE's in section 9.2 with a user prescribed tolerance of $\epsilon = 10^{-12}$.

	N_{tot}	N	T_{build} (seconds)	T_{solve} (seconds)	R (MB)
Constant convection	455233	44352	21.04	0.85	683.25
	1815681	174720	176.09	3.47	2997.80
	7252225	693504	980.93	13.76	8460.94
	28987905	2763264	5227.52	77.03	48576.75
Variable Helmholtz	114465	11424	4.61	0.19	167.68
	455233	44352	42.72	1.110	774.34
	1815681	174720	450.68	4.54	3678.31
	7252225	693504	3116.57	17.64	15658.07
Diffusion convection	455233	44352	28.31	0.795	446.21
	1815681	174720	131.23	3.20	2050.20
	7252225	693504	906.11	17.12	8460.94
	28987905	2763264	4524.99	66.99	47711.17

9.2. Convergence for unknown solutions. In this section, we apply the direct solver to three problems for which we do not know an exact solution.

Constant convection: Let the convection in the x_2 direction be constant by setting $c_1(\boldsymbol{x}) = 0$, $c_2(\boldsymbol{x}) = -100000$, and set $c(\boldsymbol{x}) = 0$.

Diffusion-Convection: Introduce a divergence free convection by setting $c_1(\boldsymbol{x}) = -10000\cos(4\pi x_2)$, $c_2(\boldsymbol{x}) = -10000\cos(4\pi x_1)$, and $c(\boldsymbol{x}) = 0$.

Variable Helmholtz: Consider the variable coefficient Helmholtz problem where $c_1(\boldsymbol{x}) = 0$, $c_2(\boldsymbol{x}) = 0$, $c(\boldsymbol{x}) = \kappa^2(1 - (\sin(4\pi x_1)\sin(4\pi x_2))^2)$, and $\kappa = 640$.

For the three experiments, the boundary data are given by $f(\boldsymbol{x}) = \cos(2x_1)(1 - 2x_2)$.

To check for convergence, we postprocess the solution as described in section 5.3 to get the solution on the Chebyshev grid. Let u^N denote the solution on the Chebyshev grid. Likewise, let u_n^N denote the normal derivative on the boundary at the Chebyshev boundary points. We compare the solution and the normal derivative on the boundary pointwise at the locations

$$\hat{\boldsymbol{x}} = (0.75, 0.25) \quad \text{and} \quad \hat{\boldsymbol{y}} = (0.75, 0),$$

respectively, via

$$E_{\text{int}}^N = |u^N(\hat{\boldsymbol{x}}) - u^{4N}(\hat{\boldsymbol{x}})| \quad \text{and} \quad E_{\text{bnd}}^N = |u_n^N(\hat{\boldsymbol{y}}) - u_n^{4N}(\hat{\boldsymbol{y}})|.$$

The tolerance for the compressed representations is set to $\epsilon = 10^{-12}$. Table 2 reports the pointwise errors. We see that high accuracy is obtained in all cases, with solutions that have ten correct digits for the potential and about seven correct digits for the boundary flux.

The computational costs of the computations are reported in Table 5. The memory R reported now includes the memory required to store all local solution operators described in section 5.3.

10. Conclusions and extensions. We have described a direct solver for variable coefficient elliptic PDEs in the plane, under the assumption that the solution and all coefficient functions are smooth. For scalar problems with nonoscillatory solutions such as the Laplace equation, the solver has an experimentally verified $O(N)$ asymptotic complexity, with a small constant of proportionality. We expect similar performance for closely related problems with nonoscillatory solutions such as, e.g.,

the Stokes equation, or the equations of linear elasticity. For problems with oscillatory solutions, high practical efficiency is retained for problems of size up to several hundred wavelengths.

Our method is based on a composite spectral discretization. We use high-order local meshes (typically of size 21×21) capable of solving even very large scale problems to ten correct digits or more. The direct solver is conceptually similar to the classical nested dissection method [7]. To improve the asymptotic complexity from the classical $O(N^{1.5})$ to $O(N)$, we exploit internal structure in the dense "frontal matrices" at the top levels in a manner similar to recent work such as, e.g., [2, 8, 16, 17, 22]. Compared to these techniques, our method has an advantage in that high-order discretizations can be incorporated without compromising the speed of the linear algebra. The reason is that we use a formulation based on DtN operators. As a result, we need high-order convergence *only in the tangential direction* on patch boundaries.

The direct solver presented requires more storage than classical iterative methods, but this is partially offset by the use of high-order discretizations. More importantly, the solver is characterized by very low data movement. This appears to make the method particularly well suited for implementation on parallel machines with distributed memory, although this has not yet been verified experimentally.

While the current manuscript treats only simple square domains, it is relatively easy to extend the methodology to domains in two dimensions (2D) that can be mapped to a rectangle, or a union of rectangles using smooth parameterizations; see, e.g, [19, sections 6.3 and 6.4]. The extension to three dimensions is in principle straightforward, but will of course require substantial work. Memory constraints become far more limiting than for problems in 2D, but initial numerical experiments indicate that fairly large problems can be handled on personal workstations. This is work in progress, and will be reported at a later date.

The method presented is designed to be particularly competitive for high-order discretizations of problems with smooth solutions. Local deviations from smoothness due to, say, a corner, or a concentrated load, can be handled using mesh refinement, but for problems with low overall smoothness in the solution, existing linear complexity direct solvers (e.g., [2, 8, 16, 17, 22]) are likely to perform better.

REFERENCES

[1] S. Chandrasekaran and M. Gu, *A divide-and-conquer algorithm for the eigendecomposition of symmetric block-diagonal plus semiseparable matrices*, Numer. Math., 96 (2004), pp. 723–731.

[2] S. Chandrasekaran, M. Gu, X.S. Li, and J Xia, *Fast algorithms for hierarchically semiseparable matrices*, Numer. Linear Algebra Appl., 17 (2010), pp. 953–976.

[3] Y. Chen, *A fast, direct algorithm for the Lippmann-Schwinger integral equation in two dimensions*, Adv. Comput. Math., 16 (2002), pp. 175–190.

[4] Y. Chen, *Total Wave Based Fast Direct Solver for Volume Scattering Problems*, preprint, arXiv:1302.2101, 2013.

[5] T.A. Davis, *Algorithm* 832: *Umfpack v*4.3*—an unsymmetric-pattern multifrontal method*, ACM Trans. Math. Software, 30 (2004), pp. 196–199.

[6] I.S. Duff, A.M. Erisman, and J.K. Reid, *Direct Methods for Sparse Matrices*, Clarendon Press, Oxford, 1989.

[7] A. George, *Nested dissection of a regular finite element mesh*, SIAM J. Numer. Anal., 10 (1973), pp. 345–363.

[8] A. Gillman, *Fast Direct Solvers for Elliptic Partial Differential Equations*, Ph.D. thesis, University of Colorado at Boulder, Boulder, CO, 2011.

[9] A. Gillman, A. Barnett, and P.G. Martinsson, *A spectrally accurate direct solution technique for frequency-domain scattering problems with variable media*, BIT, (2014).

[10] A. Gillman, P. Young, and P.G. Martinsson, *A direct solver with $o(n)$ complexity for integral equations on one-dimensional domains*, Front. Math. China, 7 (2012), pp. 217–247.

[11] L. Greengard, D. Gueyffier, P.G. Martinsson, and V. Rokhlin, *Fast direct solvers for integral equations in complex three-dimensional domains*, Acta Numer., 18 (2009), pp. 243–275.

[12] K.L. Ho and L. Greengard, *A fast direct solver for structured linear systems by recursive skeletonization*, SIAM J Sci. Comput., 34 (2014), pp. A2507–A2532.

[13] A.J. Hoffman, M.S. Martin, and D.J. Rose, *Complexity bounds for regular finite difference and finite element grids*, SIAM J. Numer. Anal., 10 (1973), pp. 364–369.

[14] B.N. Khoromskij and G. Wittum, *Numerical solution of elliptic differential equations by reduction to the interface*, Lect. Notes Comput. Sci. Eng. 36, Springer, Berlin, 2004.

[15] D.A. Kopriva, *A staggered-grid multidomain spectral method for the compressible Navier-Stokes equations*, J. Comput. Phys., 143 (1998), pp. 125–158.

[16] S. Le Borne, L. Grasedyck, and R. Kriemann, *Domain-decomposition based $\mathcal{H}$-LU preconditioners*, in Domain Decomposition Methods in Science and Engineering XVI, Lect. Notes Comput. Sci. Eng. 55, Springer, Berlin, 2007, pp. 667–674.

[17] P.G. Martinsson, *A fast direct solver for a class of elliptic partial differential equations*, J. Sci. Comput., 38 (2009), pp. 316–330.

[18] P.G. Martinsson, *A Composite Spectral Scheme for Variable Coefficient Helmholtz Problems*, preprint, arXiv:1206.4136, 2012.

[19] P.G. Martinsson, *A direct solver for variable coefficient elliptic PDEs discretized via a composite spectral collocation method*, J. Comput. Phys., 242 (2013), pp. 460–479.

[20] P.G. Martinsson and V. Rokhlin, *A fast direct solver for boundary integral equations in two dimensions*, J. Comput. Phys., 205 (2005), pp. 1–23.

[21] H.P. Pfeiffer, L.E. Kidder, M.A. Scheel, and S.A. Teukolsky, *A multidomain spectral method for solving elliptic equations*, Comput. Phys. Comm., 152 (2003), pp. 253–273.

[22] P.G. Schmitz and L. Ying, *A fast direct solver for elliptic problems on general meshes in $2d$*, J. Comput. Phys., 231 (2012), pp. 1314–1338.

[23] Z. Sheng, P. Dewilde, and S. Chandrasekaran, *Algorithms to solve hierarchically semi-separable systems*, in System Theory, the Schur Algorithm and Multidimensional Analysis, Oper. Theory Adv. Appl. 176, Birkhäuser, Basel, 2007, pp. 255–294.

[24] L.N. Trefethen, *Spectral Methods in MATLAB*, Software Environ. Tools, SIAM, Philadelphia, 2000.

[25] E.L. Wilson, *The static condensation algorithm*, Internat. J. Numer. Methods Engrg., 8 (1974), pp. 198–203.

[26] J. Xia, S. Chandrasekaran, M. Gu, and X.S. Li, *Superfast multifrontal method for large structured linear systems of equations*, SIAM J. Matrix Anal. Appl., 31 (2010), pp. 1382–1411.

[27] B. Yang and J.S. Hesthaven, *Multidomain pseudospectral computation of Maxwell's equations in 3-d general curvilinear coordinates*, Appl. Numer. Math., 33 (2000), pp. 281–289.